Applied Acoustics 235 (2025) 110657

Contents lists available at ScienceDirect

Applied Acoustics

journal homepage: www.elsevier.com/locate/apacoust

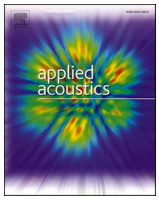

Acoustic observations of a prescribed burn☆

Omar Marcillo [a,*], Jonathan M. Lees [b], Kara Yedinak [c], Keith Bourne [c], Brian Potter [d], Steven Flanagan [e], Joseph O'Brien [e], Joseph Paki [f]

[a] Nuclear Nonproliferation Division, Oak Ridge National Laboratory, Oak Ridge, TN 37830, USA
[b] Department of Earth, Marine, Environmental Sciences, University of North Carolina at Chapel Hill, Chapel Hill, NC 27599, USA
[c] Forest Products Laboratory, USDA Forest Service 1 Gifford Pinchot Drive, Madison, WI 53726, USA
[d] Pacific Wildland Fire Sciences Laboratory, USDA Forest Service, 400 N 34th Street, #201, Seattle, WA 98103, USA
[e] Disturbance and Prescribed Fire Laboratory, USDA Forest Service, Southern Research Station, 320 Green Street, Athens, GA 30602, USA
[f] Michigan Tech Research Institute, Ann Arbor, MI 48105 USA

ARTICLE INFO

Keywords:
Infrasound
Wildfires
Combustion noise

ABSTRACT

Audible sound is known to originate from wildland fires. We show audible sound is accompanied by infrasound emissions, originating from the active combustion zone in a prescribed fire. We collected data from one of multiple prescribed burns conducted at Eglin Airforce Base, Florida in March of 2023. Single-unit infrasonic sensors and a six-element array were deployed outside the burn unit to capture acoustic signals. The array was configured as a hexagon with aperture of ~10 m. Dual-band radiometers were deployed inside the unit to track the fire's evolution. A broadband signal is observed by all infrasound sensors with variable intensity and frequency content between 2 Hz and up to 90 Hz. The sensor closest to the perimeter of the unit detected frequencies up to 90 Hz for a few minutes. Array analysis shows a coherent broadband signal with frequencies between 2 and 40 Hz emanating from the burn unit that we argue is sound from the active combustion zone. The estimated azimuths follow the ignition pattern with delays of several minutes between the ignition and detection of sound. We discuss the potential for using acoustic measurements to study the spatial and temporal evolution of fire and extract spectral features of vegetation type-specific heat release rates. Extracting fire characteristics and dynamics using sound may complement other more established measurements by providing continuous data remotely that are not constrained to line-of-sight or visibility conditions that can be affected by smoke or topography.

1. Introduction

Processes that develop unsteady energy release to the atmosphere induce a mechanical response, resulting in sound, such as in the case of volcanic and chemical explosions, earthquakes, and bolides. Low-frequency sound and infrasound (sound with a frequency below ~ 20 Hz) display low attenuation and can propagate over long distances. Combustion is included in these non-steady energetic events with the potential to generate sound [1]. Early work on combustion noise was largely limited to premixed fuel-oxygen scenarios. These efforts suggest that sound is generated by fluctuations in the rate of expansion of gases during combustion [2]. The wave equation [1] that describes the generation of sound from the unsteady release of heat can be defined by:

$$\frac{1}{c^2}\frac{\partial^2 p'}{\partial t^2} - \Delta p' = \frac{(\gamma - 1)}{c^2}\frac{\partial \dot{q}}{\partial t} \tag{1}$$

where p' is the pressure above mean, γ the ratio of specific heat capacities, c is the speed of sound in the far field, and $\dot{q}$ the heat release rate per unit volume. The far-field solution at a distance r and time t can be written as

☆ This manuscript has been authored by UT-Battelle, LLC, under contract DE-AC05-00OR22725 with the USDepartment of Energy (DOE). The US government retains and the publisher, by accepting the article for publication,acknowledges that the US government retains a nonexclusive, paid-up, irrevocable, worldwide license to publish orreproduce the published form of this manuscript, or allow others to do so, for US government purposes. DOE willprovide public access to these results of federally sponsored research in accordance with the DOE Public Access Plan(http://energy.gov/downloads/doe-public-access-plan).

* Corresponding author.
E-mail address: marcillooe@ornl.gov (O. Marcillo).

https://doi.org/10.1016/j.apacoust.2025.110657
Received 15 November 2024; Received in revised form 2 March 2025; Accepted 3 March 2025
Available online 11 March 2025
0003-682X/

$$p'(r,t) = \frac{1}{4\pi r}\frac{(\gamma-1)}{c^2}\frac{\partial \dot{Q}_{t,t-\tau}}{\partial t} \quad (2)$$

where $\dot{Q}_{t,t-\tau} = \int \dot{q}_{t-\tau} dV$ is the total heat release rate and τ is the retardation time [3,4]. For a compact source, $\dot{Q}_{t,t-\tau}$ measures the total heat release rate, which is the summed contribution of small source elements inside a flame volume. The mean acoustic power is often used to study the intensity of combustion [5]:

$$\overline{p'^2}(r,t) = \left[\frac{(\gamma-1)}{4\pi r c^2}\right]^2 \overline{\frac{\partial \dot{Q}_{t,t-\tau}}{\partial t}\frac{\partial \dot{Q}_{t,t-\tau}}{\partial t}} \quad (3)$$

A general spectral shape for acoustic power, which can be related to heat release rate, has been established based on empirical data. This shape is characterized by a spectral peak at a peak frequency (f_{peak}) and two coefficients, β and α, that control the low and high frequencies as f^{β} and $f^{-\alpha}$, respectively [6]. f_{peak} between 200 and 1,000 Hz have been observed in experiments with burners under different configurations of burner geometry, flow velocities, and turbulence intensities [7]. Other sources of combustion noise, such as buoyant flow instabilities, have been proposed with significantly lower frequencies (<10 Hz) [8,9]. These other potential noise sources were studied using controlled static fire pools and identified quasi periodic signals with frequencies controlled by the pools' geometry. Past research on the temporal and spectral characterization of combustion noise mainly used stationary and compact sources. For example in a recent study Johnson et al. [10] documented the characteristic of infrasound generated by a compact wood fire pile and associated to flame flickering. The noise from more complex and dynamic sources, such as wildland fires (e.g., wildfires or prescribed fire – referred to here as [RxF]), has not been extensively investigated because of the complexity of the environment and processes involved.

Wildfires and RxF are disturbance events that involve different fuels and terrains and exhibit a variety of active sources distributed in space. RxF are fires that are intentionally lit to meet land management objectives, and they are an important tool in forest management because they can reduce the accumulation of dead leaves, tree limbs, and other debris to prevent wildfires, restore ecosystems, and enable the growth of fire-dependent species [11]. RxFs are carefully planned and executed so fires are contained to limited areas and burn with targeted fire behavior characteristics. These fires are different from wildfires because they are conducted during periods of more predictable atmospheric conditions. Ignition of RxFs typically occurs by personnel on aerial or ground vehicles, or on foot. RxFs and wildfires are not static, and their fire behavior depends on vegetative fuels, weather, and topography. Wildfires and RxF can cover large areas and be active during different time scales. The energy released by fire is an important quantity to estimate for fire characterization. Kremens et al. [12] described the concept of radiated energy to be an analog to the energy field. The radiated energy is significant as it can be estimated using remote sensing techniques [13]. Two quantities have been introduced to quantify radiated energy: a) Fire Radiative Power (FRP) and b) Fire Radiative Energy (FRE) [13]. FRP is related to the rate of energy from fire and FRE the total energy radiated by the fire. We defined FRP as:

$$FRP = \varepsilon \cdot \sigma \cdot T^4 \quad (4)$$

where T is the temperature (K), ε is the emissivity (assumed to be 0.98) [14], and $\sigma = 5.67 \times 10^{-8}$ (W m^{-2} K^{-4}) is the Stefan-Boltzmann constant, FRP is in units of kilowatts per square meter (kW/m^2). FRE is calculated by integrating the FRP curve. Pairing acoustic observations of fires with these established radiant energy remote sensing techniques could yield otherwise unknown second and third order details of the total heat released. Likewise, acoustic emissions marry the heat release rate characteristics to the combustion characteristics of the vegetation and resultant fire behavior.

This study investigates the potential of using acoustic measurements to extract source characteristics from RxF from outside of the burning area. In March 2023, a suite of multiple acoustic sensors was deployed around an area scheduled for an RxF at Eglin Air Force Base, Florida, where a signal-rich acoustic wavefield was captured. A series of radiometers were also deployed within the burning to track the evolution of the fire. In this article, the field site and sensor configuration and the wavefield and analysis methods are described, followed by the analytical results of the analysis of infrasound data and discussion of characteristics and limitations of the acoustic approach for wildfire studies.

2. Data and methods

2.1. Burn area description and instrumentation

The ~ 5.5 km^2 burn area (G25a), was located at Eglin Air Force Base, Florida. This unit was predominantly mixed forest with small sections of long leaf pine trees and wooded wetlands. G25a was naturally partitioned on the North, South, and West by roads and to the East by Live Oak Creek [Fig. 1a]. G25a was burned on March 11, 2023 using a combination of aerial and ground ignition of strip head fires. Weather during the burn as collected from an onsite fire weather station indicated an average air temperature of 20° C, RH of 44 %, and a mean 2 m wind speed of 1 ms^{-1} from the SSE with gusts up to 4 ms^{-1}. Twenty-six dual-band radiometer sensors were deployed inside G25a [Fig. 1(a) sensors A thru Z]. In Fig. 1, radiometer stations are named (i. e., A to Z) following the progression of time for peak amplitude at each radiometer. The radiometers had a sampling rate of 1 sps and were stored in protective metal cases that were attached to poles ~ 7 m above and pointed nadir to the fuel bed.

Three infrasound stations were deployed: ST, EG, and DC—with six, three, and two sensors, respectively [Fig. 1(a) and sensor distribution in (c)]. Station ST was configured as a six-element array in a hexagon with ~ 8 m between opposite vertices. This array used infraBSU sensors [15,16] and a Centaur digitizer (Nanometrics Inc.) recording at 2,000 samples per second (sps). Station EG had three sensors, but one node was operational for only 20 min near the end of the burn. Station DC had two sensors separated by ~ 8 m. EG and DC used six-channel RT130 reftek digitizers (reftek.com) sampled at 500 sps. For the analysis presented here we are using only one sensor per station for stations EG and DC.

The fire was initiated by 5 all-terrain vehicles (ATVs) moving as a convoy. The ATVs were fitted with drip torches using a 50:50 mixture of diesel and gasoline for fuel. The ATVs were also equipped with GPS receivers and recorded location and time stamps of torch operation. Fig. 1(c) shows the ignition pattern. The fire started north of the section. The ATVs moved first along Rd.235 to the intersection of Rd 235 and Rd 253 (Fig. 1a) and entered the unit close to radiometer A from Rd 253 and then moved northeast parallel to 235. The front of the fire propagated a total of ~ 2.1 km to the southeast. ATV ignition began at 18:10 UTC and ended at 19:47 UTC. This field site was in Central Standard Time (CST) for this time of the year, and it was 6 h behind UTC. A helicopter was present during the experiment, making circular passes above the unit during the burn [Fig. 1(b)]. This helicopter was deployed to monitor the burn. We summarize here the operational characteristics of the helicopter but describe their significance for noise generation in the sub section Characteristics of the Acoustic wavefield.The helicopter was a Bell Long-Range with: 1) two blades for the main rotor with operational constant angular speed of 400 revolutions per minute (rpm) (41.88 rad/s or 6.665 Hz) and 2) two blades for the tail rotor with angular speed of 2,500 rpm (261 rad/s or 41.666 Hz).

2.2. Characteristics of the acoustic wavefield

Fig. 2 shows waveform data for one sensor from each station and the corresponding spectrogram. The waveforms at the three stations show amplitudes within ± 1 Pa. There are two main spectral features around

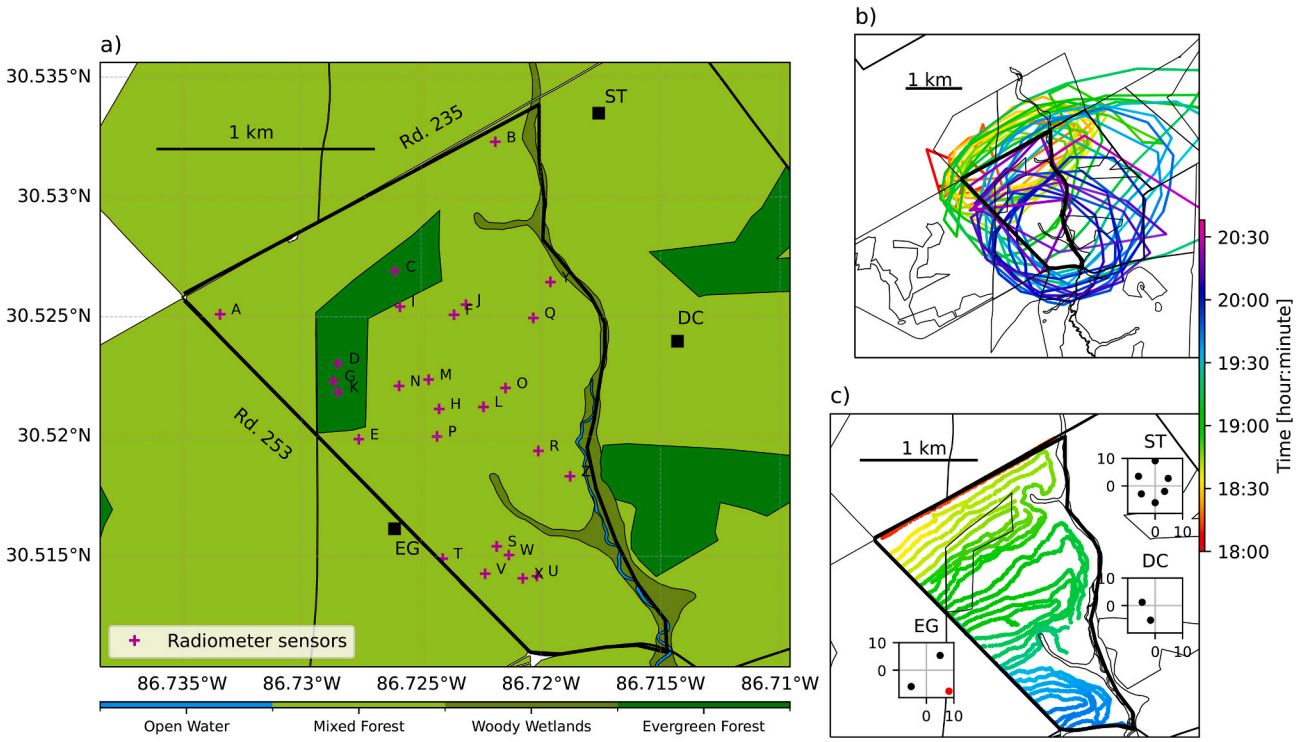

Fig. 1. (a) Map of the burning unit (G25a), outlined in black, and vegetation type. Magenta crosses show the locations of radiometers and black squares for the stations. (b) Path of the helicopter, based on on-board GPS measurements. Note that the scale in this map changed to include the general movement of the helicopter. (c) Pattern of ATV ignition, based on on-board GPS measurements. Sensor distributions are shown in the inset maps (insets' axes are in meters). The sensor in red (panel c) in station EG was only operational the last 20 min.

the time of the burn: a) spectrally discrete harmonic noise (tonal noise) and b) faint emergent broadband signals. The harmonic noise and broadband components of the wavefield are assumed to be rotor noise from the helicopter and combustion noise, respectively. Noise associated with helicopters and other rotor-based aerial vehicles is well-understood and characterized by harmonic noise in the infrasonic and low frequency acoustic band (<1000 Hz) [17]. The helicopter signals are the series of persistent oscillating horizontal lines. The fundamental frequency of this harmonic noise is related to the rate of rotation of the rotors [14] and modified by Doppler effect [18]. Two harmonic sequences (a fundamental frequency and a series or multiple integer harmonics) can be observed in the three stations. These sequences have fundamental frequencies between 11 and 15 Hz and 19 to 21 Hz, for the first and second sequences respectively. The first sequence is stronger than the second one. The broadband signal can be also observed in all stations. However, the signal is weak and has variable spectral content. At station EG the signal seems to be stronger and reaches frequencies of up to 80–90 Hz for several minutes. We study the emergence and temporal evolution of this broadband signal by using features of the acoustic field and associating that to observations of the radiometers using Equation (3). Given the prevalence and high amplitude of the harmonic noise in our data, we start our analysis by spectrally removing helicopter noise the waveforms.

2.3. Removing helicopter noise

The signals from the helicopter are the most persistent acoustic feature during the experiment. These signals can be seen in the three stations between around 18:05 (few minutes before the start of the ignition 18:10) and 20:25 (almost 40 min after the end of ignition at 19:47). These signals are seen in the spectrograms as harmonic noise with changing fundamental frequencies between 11 and 15 Hz and the corresponding harmonics. The fundamental frequency and its harmonics changed with time and depended on the relative velocity of the helicopter with respect to each station. To study the signals related to combustion noise, we first detect, characterize, and then remove the helicopter noise at each station. The detection starts by estimating the power spectral density (PSD) for short data intervals. We used a 10 s window and 50 % overlap. A Blackman-Harris window (Harris, 1978) is applied to reduce spectral leakage. The scipy routine *find_peaks* [19] is used on the PSDs for peak identification. The routine is configured to detect spectral peaks if the separation is higher than 10 Hz and the ratio between peak and base amplitudes is higher than 2. We used 10 Hz separation to avoid detections between 19 and 21 Hz related to tail rotor noise or interaction of main and tail rotors. The tail rotor harmonic sequence has peaks with significantly smaller amplitudes, and the routine sometimes does not trigger detections for this sequence. The results of the harmonic detection show clear harmonic noise with fundamental frequencies between 13.3 ± 2 Hz and up to the 6th harmonic. These fundamental frequencies correspond to the operational characteristics of the helicopter (i.e., two blades and 400 rpm) and the speed of the helicopter during the burn. The deviations from the 13.3 Hz are related to Doppler effect. These detections are used to remove the spectral peaks from the PSDs. This analysis followed a similar approach to Mann and Lees [20]. A 0.5 Hz section of the PSDs before and after a detected peak is removed. Then, a 2 Hz section before and after the removed peak is used to interpolate the removed region using a one-dimensional smoothing spline algorithm [21]. After removing and replacing the harmonic noise from the helicopter, a modified spectrogram is constructed for each station. These modified spectrograms are used for studying the energy evolution of the broadband signal. The modified spectrograms were integrated between 2 and 100 Hz to estimate acoustic power of the broadband signal. Fig. S1 in the Supplementary Material shows an example of the detection and modification of a PSD from station ST.

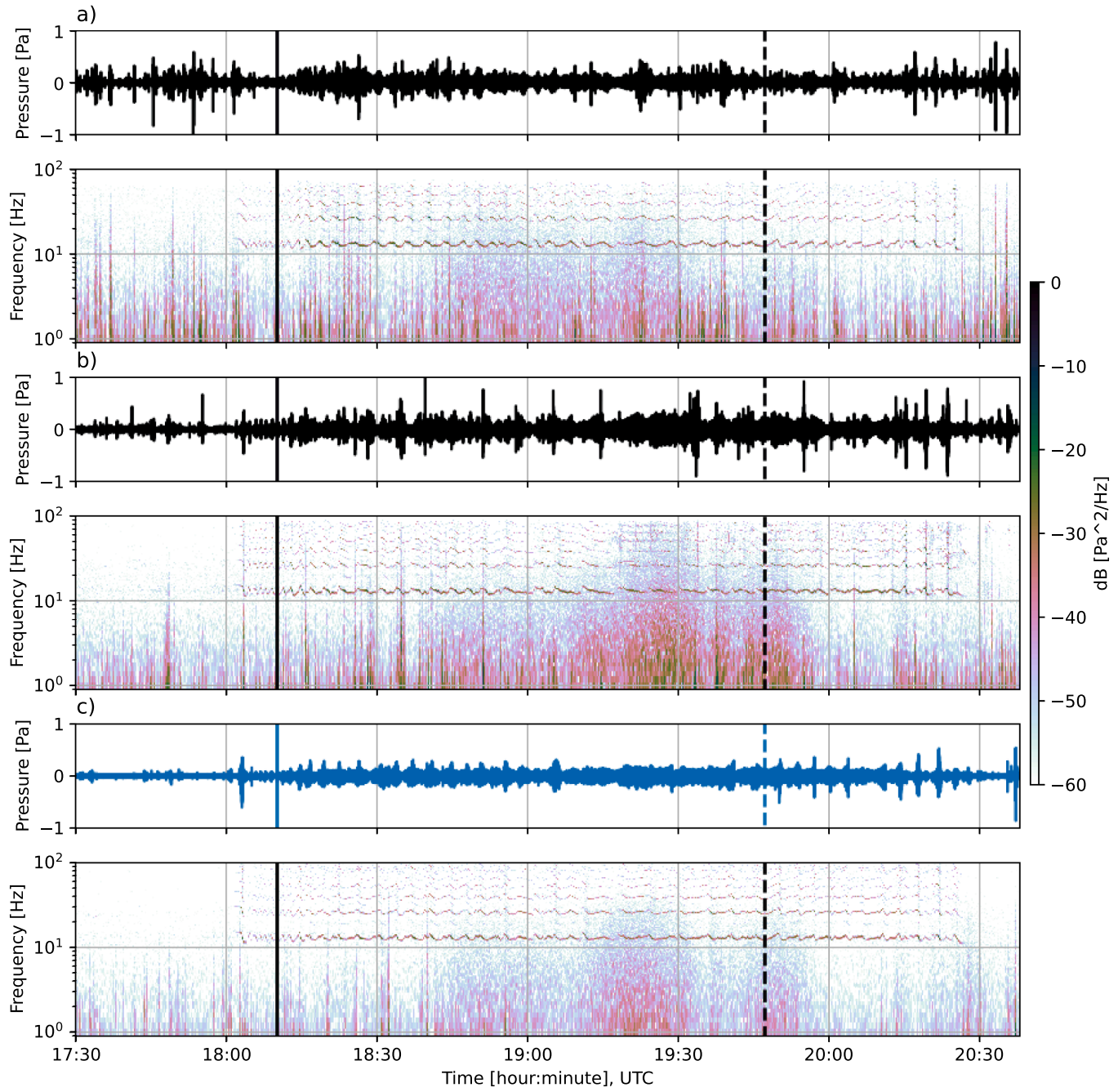

Fig. 2. Waveforms and corresponding spectrograms of one sensor are shown for each station (decibels are relative to 1 Pa): a) ST, b) EG, and c) DC. The time corresponds to the hours of March 11th, 2024. The solid and dashed vertical lines at 18:10 and 19:47 UTC show the time for the start and end of the ignition. The waveforms show a slight increase in pressure with the arrival of the helicopter to the burning area. The helicopter noise can be seen starting a few minutes after 18:00 UTC and stopping around 20:25 UTC when the helicopter left the area.

2.4. Array processing

In the analysis, we assume signals propagate horizontally with apparent speed, v, from a source at a back-azimuth (θ). The F-k method [22–24] is used in our analysis. This method uses the cross-power spectral density matrix (S) to construct a spectrum $P_f = P(S_f, v, \theta)$ and finds the combination of parameters that maximizes the power of P. This analysis is done in the frequency domain to better assess and minimize the influence of the helicopter noise in the data. In our analysis, the multichannel data are represented by the vector $\boldsymbol{x} = [x^1, \cdots, x^M]$, where M is the number of channels (number of sensors). We also define τ as the sampling interval ($\tau = 1/f_s$), and f_s is the sampling rate. The discrete Fourier Transform of a window with Q samples for the j-th channel x^j is defined as:

$$y^j(f) = \frac{1}{N\tau}\sum_{q=0}^{Q-1} w_q x^j(q\tau) e^{-i2\pi f q\tau} \tag{5}$$

where w is a window (taper) of length Q. $S(f)$ is defined as

$$S_{jk}(f) = y^j(f)^* y^k(f) \tag{6}$$

Where * is the complex conjugate operator. We estimate S_{jk} by averaging L consecutive windows as:

$$\widehat{S}_{jk}(f) = \sum_{l=1}^{L} \widehat{S}_{jk}^{l} \Big/ L \tag{7}$$

Then, P is defined as:

$$P(f, v, \theta) = a_f^*(v, \theta)\widehat{S}_{jk}(f)a_f(v, \theta) \tag{8}$$

here the vector $a_f(v, \theta) = e^{i2\pi fB}$ is a steering vector. $B = B(v, \theta)$ is a set of time delays for a signal that arrives at each station and moves with speed v and direction θ. For each frequency, we evaluate P and identify the θ and v that maximize the spectrum. At the maximum value of P, we can find the degree of correlation of the signals in the beam and use that to estimate the strength of the beam. We generate for each analyzed window and for each frequency three parameters: v, θ, and mean cross-correlation.

3. Results

The broadband signal shows a frequency range that changes with time and is station specific (Fig. 2). For the three stations the lower frequency limit is between 2 and 5 Hz. The upper frequency limit changes with stations but at around 19:20 the three stations reached the maximum frequency, i.e., around 40 Hz for ST and DC, and around 90 Hz for EG. At the three stations, acoustic energy starts increasing with the beginning of the ignition at 18:10 UTC. The three panels in Fig. 3 show the evolution of the acoustic power across the sensor network with time (gray solid lines). To estimate power, the modified PSDs (helicopter noise removed) were integrated between 2 and 100 Hz. The estimated power varies over time, with different patterns at each station. We visually identify features in the PSDs to associate with different stages of the burn. The magenta o markers correspond to a pre-ignition time. At Station ST, two energy pulses almost equal in strength are shown at 18:50 (blue x marker) and 19:20 UTC (green square marker). In the other two stations, the 18:50 UTC pulse is not clear, but the 19:20 UTC pulse is stronger. At EG and DC, a third pulse is visible at around 19:47 UTC (black + maker and end of ignition) and continues for several minutes. These pulses seem to follow a pattern of a moving source with the same pattern as the progression of the fire (based on ATV movement). For each panel in Fig. 3, the red dashed lines show the FRP for each radiometer, divided by the square distance between the sensor and radiometer, we refer to these values as scaled FRP. Observations of the acoustic power clearly show a pattern in the evolution of the fire, but those measurements cannot provide the direction of the incoming signals. The estimation of power from a single sensor includes energy from all directions. Data from array ST are used to study the direction of these signals. The array data can be used to focus on sources located inside our study area. The multichannel data from Station ST are processed to extract the azimuthal evolution of the signals.

Fig. 4 shows the results of the array processing of Station ST. In each panel, time–frequency pixels are color-coded with back-azimuth (a), apparent speed (v), and mean cross-correlation (c). Pixels were filtered in (a) and (b) using a threshold of 0.8 from (c) mean cross-correlation and speeds between 340 and 400 m/s (b). We are using a 340 m/s lower band for the speed considering that the mean air temperature during the burn was 20° C, which corresponds to a sound speed of 343.5 m/s. The helicopter signal has high-correlation values, and the estimated azimuths change rapidly and circulate around the station. Azimuths derived from array analysis agree with the GPS-based locations reported by the helicopter. The analysis of signals from the helicopter are outside of the scope of this manuscript and are not presented here. They are mentioned primarily to suggest that the array analysis works well with respect to the helicopter signals. Derived acoustic speeds, or apparent velocities, reach values near and above 400 m/s, expected because of the proximity of the helicopter to the array, where signals arrive at high elevation angles. Furthermore, broadband signals intensify between 18:45 and 19:30 UTC. Speeds are mainly constrained below 360 m/s, and back-azimuths display a gradual, smooth

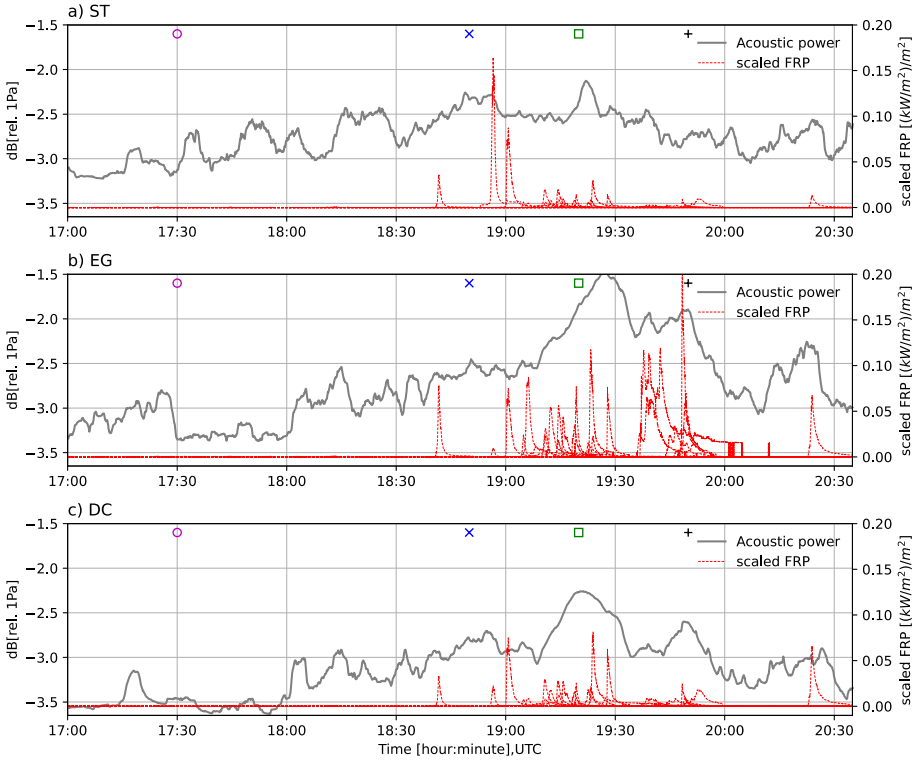

Fig. 3. The time evolution of acoustic energy of the broadband signal and FRP. Panels a, b, and c correspond to stations ST, EG, and DC, respectively. In the three plots, the acoustic power is shown in decibels that are relative to 1 Pa. Scaled FRP data are shown (in red dashed lines) for all sensors. Scale FRP is computed by diving FRP to the square of the radial distance.

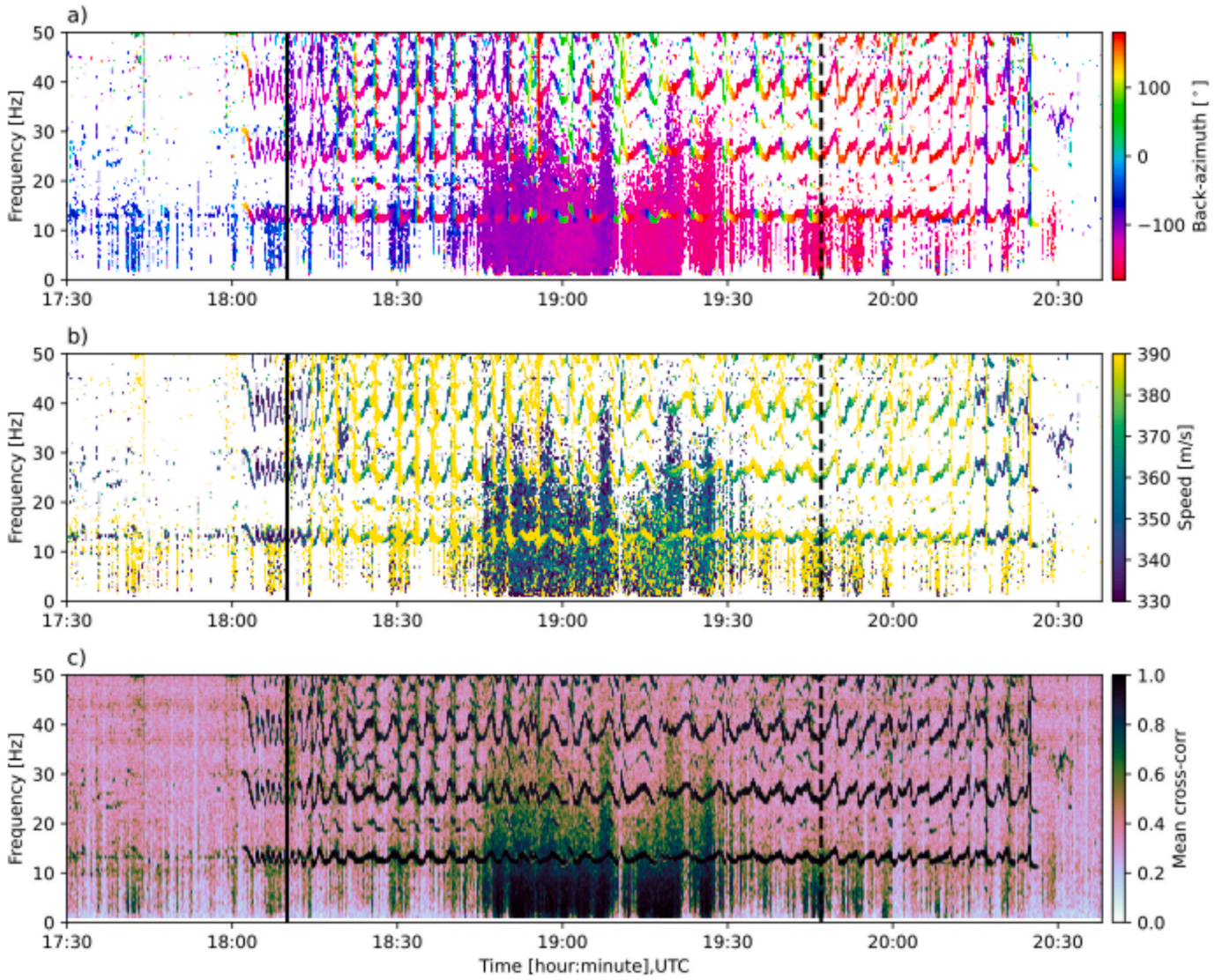

Fig. 4. Results of array processing for Station ST. (a) Estimated back-azimuth direction of incoming wave. (b) Estimated apparent speed of the acoustic wave across the array. (c) Mean cross-correlation of the array nodes vs. frequency. Oscillating high values are helicopter noise and associated higher harmonics. Vertical solid and dashed black lines correspond to the start and end of ignition, respectively.

progression, with back-azimuths between −80° and −180°, corresponding to azimuthal directions emanating from the burning unit.

While it is possible to remove some of the helicopter interference, the primary signal of interest lies in the 2–10 Hz band where we focus on possible recordings of combustion signals. The radiometer sensors [12], identified by letters A to Z, provide spatio-temporal constraints on the dynamics of the fire progression. Fig. 5(a) shows the evolution of FRP with time relative to the onset of fire contact. The temporal characteristics of the FRP show clear onsets, with heat reaching the maximum values within 1 min of the onset and several minutes for heat to return to background levels. On average sensors detected heat for a duration of 5 min. Sensors S and A have the longest detected thermal radiation, with around 19 and 24 min to reach background values, respectively. Sensors B and K display the shortest active times with around 3 and 1 min, respectively. Fig. 5(b) shows the evolution of acoustically estimated back-azimuths for the ST array. The green plus markers correspond to the average of back-azimuths azimuths between 2 and 10 Hz for one minute with the light green error bars corresponding to the standard deviation. The solid and dashed cyan lines are the back-azimuths of the top and bottom of the burn unit. The solid and dashed magenta lines correspond to the start and end of the evergreen forest patch shown in Fig. 1 (a). The blue dots correspond to back-azimuth–time location of the ATVs during ignition. The area between Rd. 235 and north part of the evergreen patch (back-azimuths between −100° and −125°) which comprises mixed forest, generates coherent energy that lasts for around 25 min, from 18:45 to 19:10 UTC. Note that at this point in the burn the ATVs have left this area and entered the back-azimuths of the evergreen region. Back-azimuth estimates between 19:10 and 19:20 UTC are constrained to the evergreen region. Note that FRP also shows that Sensors C, D, G, and K detected an increase in heat and coherent signals simultaneously.

4. Discussion

Acoustic instrumentation installed in the perimeter of unit G25 in Eglin Air Force Base during a RxF allowed researchers to characterize the acoustic wavefield during the burn. Two main components in the low frequency wavefield were identified: helicopter noise with harmonic features and a broadband signal proposed to be related to combustion processes. The helicopter signal displays discrete spectral energy and based on array processing, high coherence, apparent speed (>360 m/s), and rapid azimuth changes, which correspond to the movement of

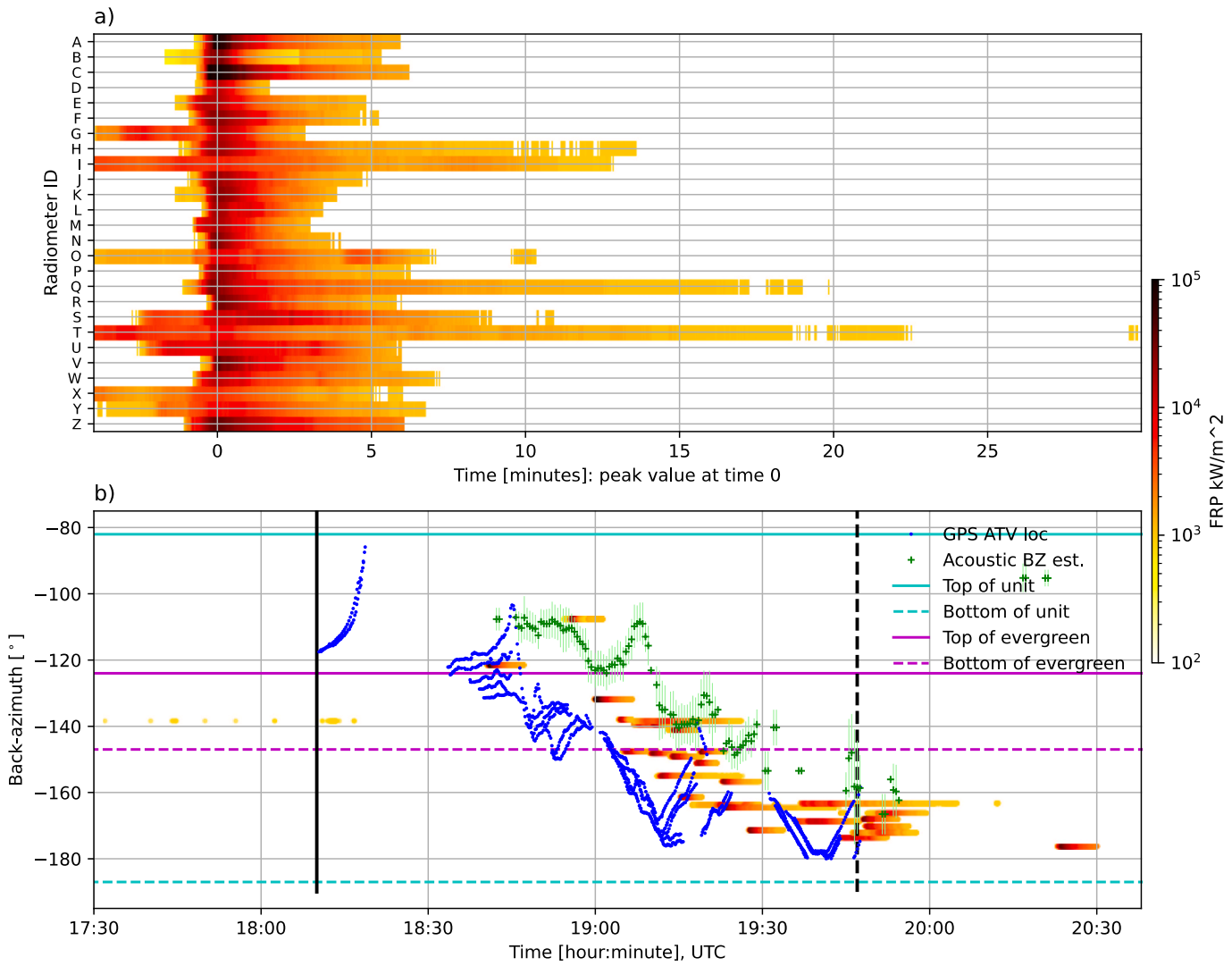

Fig. 5. A) FRP data from the radiometers listed alphabetically to correspond to map location. For each radiometer time 0 corresponds to the time of maximum FRP. b) back-azimuths estimated from acoustic data versus time. mean and error (one standard deviation) values over one minute are shown in dark green plus markers and light green lines, respectively. The average includes well-resolved back-azimuths estimated at station st for frequencies between 2 and 10 Hz. The solid and dashed cyan lines indicate back-azimuths for the top and bottom of the burn unit. The solid and dashed magenta lines correspond to the start and end of the evergreen forest region shown in Fig. 1a. The blue dots correspond to azimuth-time location of the ATVs during ignition.

the helicopter above the unit. Using these features of the helicopter noise, this component was filtered from the original PSD and used to track the evolution of the broadband signal. The acoustic power in the three stations (Fig. 3) follows a pattern of a source moving parallel to Rd. 253. Using the array data from Station ST, we constrained the signal to the burning unit and to the lower frequencies between 2 and 100 Hz. The results from array processing, along with the GPS information from the helicopter and ATVs used for ignitions, confirm that this broadband signal is not from contextual operations (Fig. 5), and the research team hypothesizes that it is related to combustion noise. Using the radiometer data, we identified times and areas that radiated heat and found coherent acoustic signals (Fig. 3 and Fig. 5). With the acoustic network, features of the power of the wavefield and azimuthal distribution of signals were discovered, and a bulk direction of movement of the combustion noise was established. However, with the instrumentation, the noise sources could not be constrained in two dimensions. To identify the location of heat sources, future deployments could use multiple arrays around areas being burned. The array analysis presented here assumed a single point heat source, but multiple sources are active at the same time at different back-azimuths (Fig. 5b). Other array techniques optimized to study multiple sources [25] could be used to analyzed sound from wildfire and RxFs and potentially track the evolution of multiple fronts or regions in burning areas simultaneously.

The radiometer network deployed at Eglin Air Force Base provided in situ measurements of the temporal evolution of heat release in areas within the fire. Some areas with active release of heat were identified as sources of acoustic energy. Equation (2) shows a direct relationship between pressure and change in total heat release rate. This can be exploited to use acoustic measurements, recorded remotely, as a proxy for total heat release rate. Having a spectral range of up to 1,000 Hz (for ST), acoustic data may be used to extend, complement, or validate other low-rate heat sensors. For example, Fig. 6 shows PSD estimates for one sensor of each station at times with peak acoustic energy (colored dots in Fig. 3) before arrival of helicopter and ignition start (magenta line), at the first pulse of energy of ST (blue line), second pulse of energy of EG (green line), and third pulse of energy at DC and the stop of ATV ignition. The highest energy levels for all sensors are at 19:20 UTC, corresponding to highly coherent signals with azimuth in the direction of the evergreen forest patch (Fig. 5). At the point of highest energy, the PSDs do not show a clear and distinct peak but rather show a more broadband increase in energy. This may be related to combinations of acoustic signals from multiple types of fuels at different radial distances.

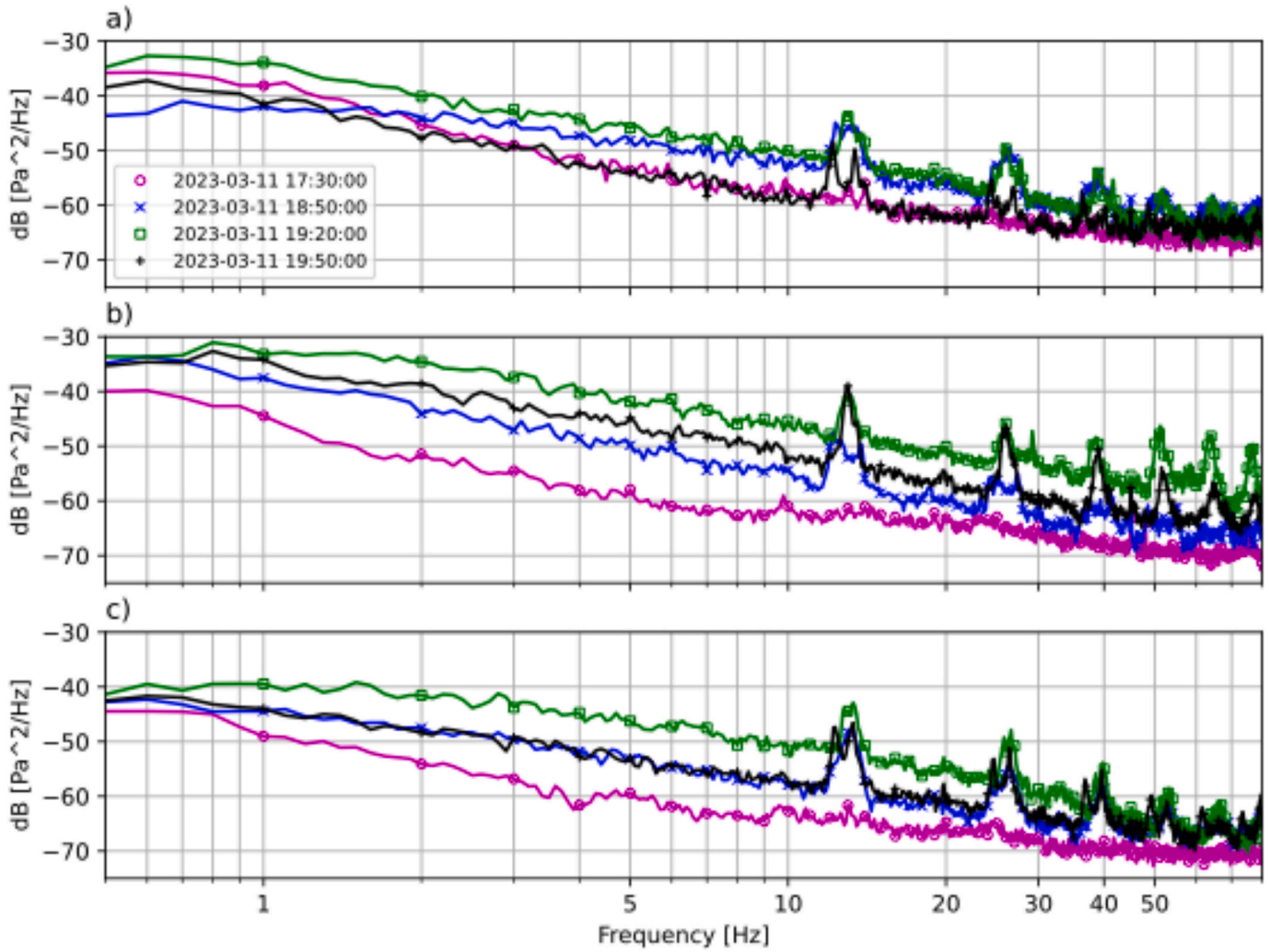

Fig. 6. Power spectral density (PSD) estimated at different times of the burn. Panels a, b, and c correspond to stations ST, EG, and DC, respectively. Before arrival of helicopter and ignition start (magenta o marker), first pulse of energy of ST (blue x marker), second pulse of energy of EG (green square marker), and third pulse of energy at DC (black + marker). The marker/color of each PSD matches the marker/color in Fig. 3. Note the spectral peaks above 10 Hz are related to helicopter noise (fundamental and multiple harmonics).

We are describing acoustic and infrasonic signals from combustion that are associated to temporal changes in the heat release rate. Large wildfires energetically modify their own environment and may generate also gravity waves by pushing large amounts of hot air upward. We suggest that some regional and global infrasound array deployments may provide means to capture infrasonic signals and gravity waves from large wildfires. For example, station IS53US in Alaska is an infrasound station of the CTBT International Monitoring System [26].The location and topology of this station can be suitable to look for signals related to gravity waves generated by large fires. There are datasets of daily growth on large fires in the western United States [27] that could be used with stations like IS53US to look for signatures from large wildfires.

5. Conclusions

Acoustic signals with low-frequency content (<100 Hz) emanating from an area during a RxF were identified. Proposed fire signals are dynamic and change in space and time. The intensity and spectral content of the signals depend on the instantaneous fire evolution and relative sensor distance. Using a sensor array, the azimuthal evolution of these signals was tracked and associated with the movement of the fire estimated by ground truth in the form of a network of radiometer sensors. The method simultaneously located the monitoring helicopter during the experiment, corroborating the array processing capabilities and allowing separation of helicopter and fire-related noises in azimuth and frequency. These first observations may provide the basis for future deployments to capture the acoustic signature of fire. Acoustic energy may provide constraints on the intensity, growth, dynamics, and geometry of the fire. Extracting fire characteristics and dynamics using sound may complement other more established measurements by providing continuous data remotely that are not constrained to line-of-sight or visibility conditions that can be affected by smoke or topography.

CRediT authorship contribution statement

Omar Marcillo: Writing – review & editing, Methodology, Investigation, Conceptualization. **Jonathan M. Lees:** Writing – review & editing, Methodology, Investigation, Conceptualization. **Kara Yedinak:** Writing – review & editing, Methodology, Investigation, Conceptualization. **Keith Bourne:** Writing – review & editing, Investigation. **Brian Potter:** Writing – review & editing, Investigation, Conceptualization. **Steven Flanagan:** Writing – review & editing, Methodology, Investigation. **Joseph O'Brien:** Methodology, Investigation. **Joseph Paki:** Methodology, Investigation.

Declaration of competing interest

The authors declare that they have no known competing financial interests or personal relationships that could have appeared to influence the work reported in this paper.

Acknowledgments

This research was sponsored in part by the Laboratory Directed Research and Development Program of Oak Ridge National Laboratory, managed by UT-Battelle, LLC, for the US Department of Energy (OM). Support for this research was provided by USDA US Forest Service award 22-JV-11111135-061 (JML). We would like to acknowledge Bob Kremens (RIT) who designed and built the dual-band radiometer sensors. We would also like to acknowledge also support from SERDP funding (RC19-1119) and the Incident Research Management Team.

Appendix A. Supplementary data

Supplementary data to this article can be found online at https://doi.org/10.1016/j.apacoust.2025.110657.

Data availability

Data will be made available on request.

References

[1] Dowling AP, Mahmoudi Y. Combustion noise. Proc Combust Inst 2015;35(1):65–100.
[2] Hurle IR, et al. Sound emission from open turbulent premixed flames. Proc Royal Soc Lond Ser A, Math Phys Sci 1968;303(1475):409–27.
[3] Swaminathan N, et al. Heat release rate correlation and combustion noise in premixed flames. J Fluid Mech 2011;681:80–115.
[4] Zhang F, et al. Combustion-generated noise: an environment-related issue for future combustion systems. Energy Technol 2017;5(7):1045–54.
[5] Liu Y. Two-time correlation of heat release rate and spectrum of combustion noise from turbulent premixed flames. J Sound Vib 2015;353:119–34.
[6] Rajaram R, Lieuwen TIM. Acoustic radiation from turbulent premixed flames. J Fluid Mech 2009;637:357–85.
[7] Kotake S, Takamoto K. Combustion noise: effects of the shape and size of burner nozzle. J Sound Vib 1987;112(2):345–54.
[8] Bedard AJ, Nishiyama RT. Infrasound generation by large fires: experimental results and a review of an analytical model predicting dominant frequencies. in IEEE International Geoscience and Remote Sensing Symposium. 2002.
[9] Cetegen BM, Ahmed TA. Experiments on the periodic instability of buoyant plumes and pool fires. Combust Flame 1993;93(1–2):157–84.
[10] Johnson JB, Anderson JF, Yedinak K. Infrasound produced by a small pile fire. Appl Acoust 2025;231:110559.
[11] Service UF. Confronting the Wildfire Crisis. 2022, U.S. Department of Agriculture.
[12] Kremens RL, Smith AMS, Dickinson MB. Fire metrology: current and future directions in physics-based measurements. Fire Ecol 2010;6(1):13–35.
[13] Lentile LB, et al. Remote sensing techniques to assess active fire characteristics and post-fire effects. Int J Wildland Fire 2006;15(3):319–45.
[14] O'Brien JJ, et al. High-resolution infrared thermography for capturing wildland fire behaviour: RxCADRE 2012. Int J Wildland Fire 2016;25(1):62–75.
[15] Marcillo O, Johnson JB, Hart D. Implementation, characterization, and evaluation of an inexpensive low-power low-noise infrasound sensor based on a micromachined differential pressure transducer and a mechanical filter. J Atmos Oceanic Tech 2012;29(9):1275–84.
[16] Slad G, Merchant BJ. Evaluation of low cost infrasound sensor packages. 2021, Sandia National Lab.(SNL-NM), Report Number: SAND2021-13632 2021;701386. https://doi.org/10.2172/1829264.
[17] Lowson MV, Ollerhead JB. A theoretical study of helicopter rotor noise. J Sound Vib 1969;9(2):197–222.
[18] Lorenz RD, et al. The sounds of a helicopter on Mars. Planet Space Sci 2023;230:105684.
[19] Virtanen P, et al. SciPy 1.0: fundamental algorithms for scientific computing in Python. Nat Methods 2020;17(3):261–72.
[20] Mann ME, Lees JM. Robust estimation of background noise and signal detection in climatic time series. Clim Change 1996;33(3):409–45.
[21] Dierckx P. A fast algorithm for smoothing data on a rectangular grid while using spline functions. SIAM J Numer Anal 1982;19(6):1286–304.
[22] Capon J. *High-resolution frequency-wavenumber spectrum analysis*. Proc IEEE 1969;57(8):1408–18.
[23] Rost S, Thomas C. ARRAY SEISMOLOGY: METHODS AND APPLICATIONS. Rev Geophys 2002;40(3):2-1–2-27.
[24] Shumway RH, Smart E, Clauter DA. Mixed signal processing for regional and teleseismic arrays. Bull Seismol Soc Am 2008;98(1):36–51.
[25] Shumway RH. Advances in mixed signal processing for regional and teleseismic arrays. Davis: University of California; 2006.
[26] Christie DR, Campus P. The IMS Infrasound Network: Design and Establishment of Infrasound Stations, in Infrasound Monitoring for Atmospheric Studies, A. Le Pichon, E. Blanc, and A. Hauchecorne, Editors. 2009, Springer Netherlands: Dordrecht. p. 29-75.
[27] Potter BE, McEvoy D. Weather factors associated with extremely large fires and fire growth days. Earth Interact 2021;25(1):160–76.